SEMARAK ILMU PUBLISHING

Journal of Advanced Research in Fluid Mechanics and Thermal Sciences

Journal homepage:
https://semarakilmu.com.my/journals/index.php/fluid_mechanics_thermal_sciences/index
ISSN: 2289-7879

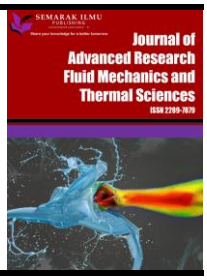

Seismic Wave Excitation of Mature Oil Reservoirs for Green EOR Technology

Mohammed Bashir Abdullahi[1], Shiferaw Regassa Jufar[1,*], Iskandar Dzulkarnain[1,2], Tareq Mohammed Al-shami[1], Minh Duc Le[3]

[1] Department of Petroleum Engineering, Universiti Teknologi PETRONAS, Malaysia
[2] Centre of Research in Enhanced Oil Recovery, Institute of Hydrocarbon Recovery, Universiti Teknologi PETRONAS, Malaysia
[3] Faculty of Transportation Mechanical Engineering, The University of Danang–University of Science and Technology, Vietnam

ARTICLE INFO

Article history:
Received 24 October 2022
Received in revised form 6 February 2023
Accepted 14 February 2023
Available online 25 February 2023

Keywords:
Elastic wave; EOR; finite element method; mesoscopic frequency; oil reservoir; seismic stress

ABSTRACT

Elastic wave-based oil mobilization of residual oil in heterogeneous reservoirs is a viable, low-cost, and green technology method of enhanced oil recovery (EOR). Applications for elastic (seismic) waves at the reservoir scale are currently in the preliminary stages of investigation and development. We employ a two-layer numerical finite element method (FEM) in this research to investigate the possibility of effective propagation of seismic waves in the low permeability area of a mature oil reservoir when seismic stress load is delivered to the rock matrix via a downhole source. The purpose of this research is to evaluate the potential of fluid and rock matrix displacement amplitudes for crossflow generation in a mature oil reservoir. In a low permeability formation, the numerical results reveal that, as the observation radius approaches the reservoir boundary, the rock matrix time-domain displacement performs better as a wave propagation parameter than the pore fluid displacement. However, crossflow oscillations at a peak mesoscopic frequency of 3.0 Hz produce an instantaneous oil transfer rate (recovery rate) of 2.5% (bypassed oil) from the low permeability area. This method can be used in combination with water flooding to recover more oil from both high and low-permeability areas. Mesoscopic attenuation frequency can therefore be utilized as one of the indicators to assess oil recovery in heterogeneous oil reservoirs.

1. Introduction

The total global energy demand for oil and natural gas energy reserves is predicted to grow in the future due to the exponential rise of the global population and the industrialization of developing economies [1-3]. The Energy Information Administration (EIA) projects a 48% increase in global energy consumption between now and 2040 [4,5]. The need for energy is still increasing despite recent advancements in renewable energy, energy efficiency, energy conservation, and the effects of COVID-19 [6]. Sustainable development goals and net zero emissions targets are established for

* *Corresponding author.*
E-mail address: shiferaw.jufar@utp.edu.my

https://doi.org/10.37934/arfmts.103.2.180196

nations since economic expansion accelerates CO_2 emissions. The achievement of sustainable development targets will depend on the transition to low-carbon fuels or renewable energy sources in the future [7,8]. One of the most difficult challenges facing the oil industry nowadays is balancing rising global energy demand while reducing greenhouse gas (GHG) emissions: world consumption is presently estimated at 100 million B/D. The most effective approach for addressing rising energy demand and reducing greenhouse gases before green energy takes the largest predicted share of the energy mix by mid-century is to implement enhanced oil recovery (EOR) technologies and scale up CCS technology [9]. The importance of EOR techniques to improve oil production from mature reservoirs has increased due to the ongoing demand for hydrocarbon sources of energy and the challenges (investment and technical) involved in the discovery and development of new oilfields [9-12]. Because of the high capillary effect and heterogeneity of oil reservoirs, less than 30-50% of the original-oil-in-place (OOIP) can be recovered by a reservoir's natural energy mechanisms, or by a combined effect of primary energy processes and water-flooding mode [13].

In addition to technical limitations specific to mature oilfields, economic factors play a significant role in determining the best EOR strategy. Hence, any EOR method that is effective, affordable, and environmentally friendly is now becoming a leading candidate for recovering residual oil in heterogeneous reservoirs [11-14]. Elastic (seismic) wave-based EOR has been observed as a potentially affordable and eco-friendly EOR technology [14,15]. According to the literature and field experiments, seismic excitation increases oil well production by 10-65% [16]. Seismic wave-based EOR techniques (Vibroseismic or Downhole technologies) have the potential to significantly vibrate oil reservoirs, releasing residual oil which may thereafter be recovered by traditional EOR processes [17]. Natural earthquakes were discovered to augment oil output by up to 45% in the 1950s when the concept originally gained traction. The use of Vibroseismic (surface) vibrators above a specific pay zone in the 1980s to replicate the impacts of natural earthquakes was generally unproductive and economically unviable. Subsurface (downhole) shockwave-generating techniques that were later developed showed more promise. The first patent for Applied Seismic Research (ASR) Corporation (downhole technology) was granted in 2000. Downhole seismic excitation is one of the greenest EOR alternatives available [15]. Seismic excitation can be used especially in combination with conventional chemical EOR techniques to optimize the areal sweep efficiency of waterflood reservoirs [11,18]. The use of seismic EOR in conjunction with polymer flooding could improve oil mobilization and recovery rates [17]. Partially hydrolyzed polyacrylamide (HPAM) polymer has demonstrated higher recovery during polymer flooding, resulting in higher sweep efficiency [19,20]. The optimum oil recovery was achieved at a higher water salinity, according to research data, which also revealed that the impact of elastic waves on oil production varied with changes in the salinity of the water injected into clayey sandstones using sandpack [21]. The injection of various chemicals in combination with seismic excitation is one of the approaches to boost its efficiency [22,23].

Residual oil is mobilized by applying compressional (P) wave excitation, which uses low-frequency and high-energy elastic waves [13,14,22]. In seismic wave-based EOR, wave sources (emitters) such as downhole/wellbore seismic vibrators, wellbore hydraulic pumps, and Vibroseismic technologies are frequently utilized for field implementation [13,16,17,24]. Elastic waves can be produced by the above-mentioned sources, either directly or indirectly. The downhole seismic excitation equipment can be placed in mature oil wells between 700-10,000 ft. It has a longevity of up to 1.5 years and normally needs no maintenance. With the use of a single device and a standard pumping system, seismic excitation can be accomplished. Oil droplets trapped in the matrix grains are displaced by seismic waves produced by the downhole system [15,25]. The reservoirs with flow obstacles in the regions of bypassed oil appear to be the best candidates for seismic excitation [26,27]. Downhole seismic waves propagate both horizontally and vertically, which causes the trapped oil droplets to be

mobilized [15,25]. This technique can also be employed as a fluid indicator to monitor wave-based EOR using SH-wave attenuation, as well as to detect and visualize permeability changes in reservoirs during CO_2 plume storage for the motive of monitoring the safety of CO_2 geo-sequestration [28]. Primarily, the elastic wave can uniformly stimulate the whole or partial area of an oil reservoir, while chemical [19] or gas flooding [13,17,27] can hardly sweep the entire oil reservoir size due to the reservoir's inherent heterogeneity [11,13,14,17,27]. Why not implement CO_2 EOR to improve oil recovery? For CO_2 EOR, large-scale infrastructure investment will be required, which energy corporations will not carry out without support from the government (authorities). The notion of the associated risk with injecting (recycling) CO_2 into depleted oil wells for EOR and huge investment in infrastructure contributes to this reticence [9]. Studies published by Kouznetsov *et al.,* [21] and Simkin and Surguchev [29] evaluate the displacement of oil by gas-free and CO_2-saturated water using elastic wave excitation. The experiments were carried out using a sandstone sandpack. The presence of elastic waves improved oil recovery in the sandpack for both cases [26].

The downhole technique works in depleted oil well, its volume coverage extends through a barrier such as fault blocks and formation layers, stimulating EOR in an oil reservoir within a radius of up to 1.4 miles [15,25]. It does not require injecting highly hazardous chemicals or fluids into the subsurface formations, nor does it deal with the by-products produced by other EOR processes. It is used in a fully closed wellbore with no hydraulic communication with the neighboring formations. It can provide some relief to field operators dealing with problems like controlling groundwater pollution from hazardous chemicals. Effectively managing the treatment, transportation, and disposal of huge quantities of wastewater effluents. Dealing with the environmental impacts of thermal injections' high energy and carbon consumption. The McKinney, Texas-based company ASR Corporation has deployed more than 200 of its innovative downhole seismic excitation technologies in more than 50 places, such as Arkansas, California, Canada, Egypt, Kansas, Mexico, Oklahoma, Oman, and Texas oilfields, etc. [15]. It has been found that seismic excitation in a broader area of a producing oil reservoir increases the production of oil while reducing the oil-water-cut ratio [11,26,23]. Moreover, enhanced oil production has been observed during field tests with wave generators operating in the low frequency (1-100 Hz) range up to 200 Hz (sonic frequency) for Vibroseismic or downhole systems, in producing or shut-in oil wells, and mature (depleted) oilfields [13]. In addition to the field findings, experimental investigations into the fundamental mechanisms of the seismic wave-based EOR technique have been evaluated [17,27]. According to the proposed primary mechanism, oil droplets trapped within the pore spaces can be mobilized by the vibration of the reservoir rock pore walls [17,27,30,31]. Pore wall displacement can mobilize, and discharge confined oil droplets into the wellbore by combining them into larger coalesced droplets. Laboratory investigations have shown that utilizing elastic or fluid-pressure wave generators (sources) at low frequencies can displace trapped oil droplets [17,27]. Beckham *et al.,* [31], Roberts and Abdel-Fattah [32] and Roberts *et al.,* [33,34] demonstrated that trapped oil droplets can be liberated by applying dynamic stress to the solid rock matrix of a sandstone core at seismic frequencies between 10 and 100 Hz. Vogler and Chrysikopoulos [35] reported that high-frequency acoustic waves (300 Hz) can liberate nonaqueous phase liquid (NAPL) from porous and permeable core samples. Oil recovery from confined sandpack can be expedited by fluid pressure vibration at a frequency range between 30 and 60 Hz, according to research by Spanos *et al.,* [36].

Moreover, Iassonov and Beresnev [37] proposed a threshold capillary trapping system that dictates how an oil droplet trapped within pore spaces should overcome the capillary force. For oil droplets trapped within the pore spaces, the elastic wave-induced inertial force must be greater than a predefined threshold limit. Further experimental studies and numerical experiments revealed that the acceleration field of the rock matrix should be between 0.1 to 10 m/s^2 or beyond to cause

mobilization of the oil droplet [30,38-41]. It was also demonstrated that the threshold acceleration amplitude depends on the background differential pressure, capillary pressure, residual oil viscosity, pore space dimension, and wave frequency. It is essential to investigate how downhole technology can adequately stimulate a hydrocarbon formation to accelerate above the residual oil's threshold mobility. It is unclear whether the pore fluid pulses or elastic waves propagating through the rock matrix generate stronger energy [17]. Stress wave vibration has been demonstrated to cause crossflow at the boundary (interface) between the high and low-permeability zones in heterogeneous or fractured oil reservoirs [17,27,23]. Elastic waves generate pore-pressure vibrations across layers of varying permeability in heterogeneous oil reservoirs [13,23,42]. The bypassed oil can be adequately recovered from the low-permeability region to the high-permeability zone using a seismic pulse [17]. In a fractured oil reservoir, the flow of bypassed oil from the matrix of the rock to the fracture can be optimized by applying appropriate hydraulic wave sources (emitters) to a fracture, which can create a periodic differential pressure between the surrounding rock matrix and the fracture [13,42]. The purpose of this study is to investigate the effectiveness of elastic wave propagation in a low-permeability layer of a heterogeneous oil reservoir. We study numerically the potential of downhole technology to stimulate reservoir-scale oil mobility (time-domain rock and fluid displacement amplitudes). We used the crossflow model proposed by Huh [23] and the multilayer poroelastic formulations of Jeong *et al.,* [17] to assess the possibility of increased oil recovery in the waterflood oil reservoir.

2. Methodology

2.1 Elastic Wave Physics

Compressional waves are generated from a downhole source and transmitted to the reservoir formations in a half-plane system (Figure 1) [14,28]. $b(m)$ denotes the radius of the oil reservoir, θ° denotes the angle of incidence of the P-waves, and $h\ (m)$ denotes the depth ratio of the reservoir. We assume the oil reservoir contains poroelastic layers (porous, permeable, and elastic) surrounded by an impermeable elastic solid formation. The partial differential equations (PDEs) govern the transmission of P-waves inside the coupled poroelastic rock-elastic solid rock model ($\Omega = (0, \mathrm{L})$) [17].

Eq. (1) defines the propagation of compressional waves through elastic solid formations. The modified Biot's coupled compressional wave model for fluid-saturated poroelastic formation layers can be mathematically expressed in Eqs. (2) and (3). Eq. (2) is the formulation of the coupled solid-fluid motion, and Eq. (3) is the modified Darcy's law in terms of the inertial forces of the coupled solid-fluid motion. x(m) represents location (position), while t(s) represents time. The boundaries between the impermeable elastic solid and the poroelastic layers are denoted by x_p and x_{p+Npls}. The index of the upper or higher permeability poroelastic layer is represented by the subscript p.

$$\frac{\partial}{\partial x}\left((\lambda + 2\mu)\frac{\partial u_a}{\partial x}\right) - \rho\frac{\partial {u^2}_a}{\partial t^2} = 0, \quad x \in \Omega\backslash\Omega_p,\ t \in (0,T), \tag{1}$$

$$\frac{\partial}{\partial x}\left((\lambda + 2\mu + \alpha^2 Q)\frac{\partial u_b}{\partial x} + \alpha Q\frac{\partial w}{\partial x}\right) - \rho\frac{\partial {u^2}_b}{\partial t^2} - \rho_f\frac{\partial^2 w}{\partial t^2} = 0, \quad x \in \Omega_p,\ t \in (0,T), \tag{2}$$

$$\frac{\partial}{\partial x}\left(\alpha Q\frac{\partial u_b}{\partial x} + Q\frac{\partial w}{\partial x}\right) - \frac{1}{k}\frac{\partial w}{\partial t} - \rho_f\frac{\partial {u^2}_b}{\partial t^2} - \frac{\rho_f}{n}\frac{\partial^2 w}{\partial t^2} = 0, \quad x \in \Omega_p,\ t \in (0,T), \tag{3}$$

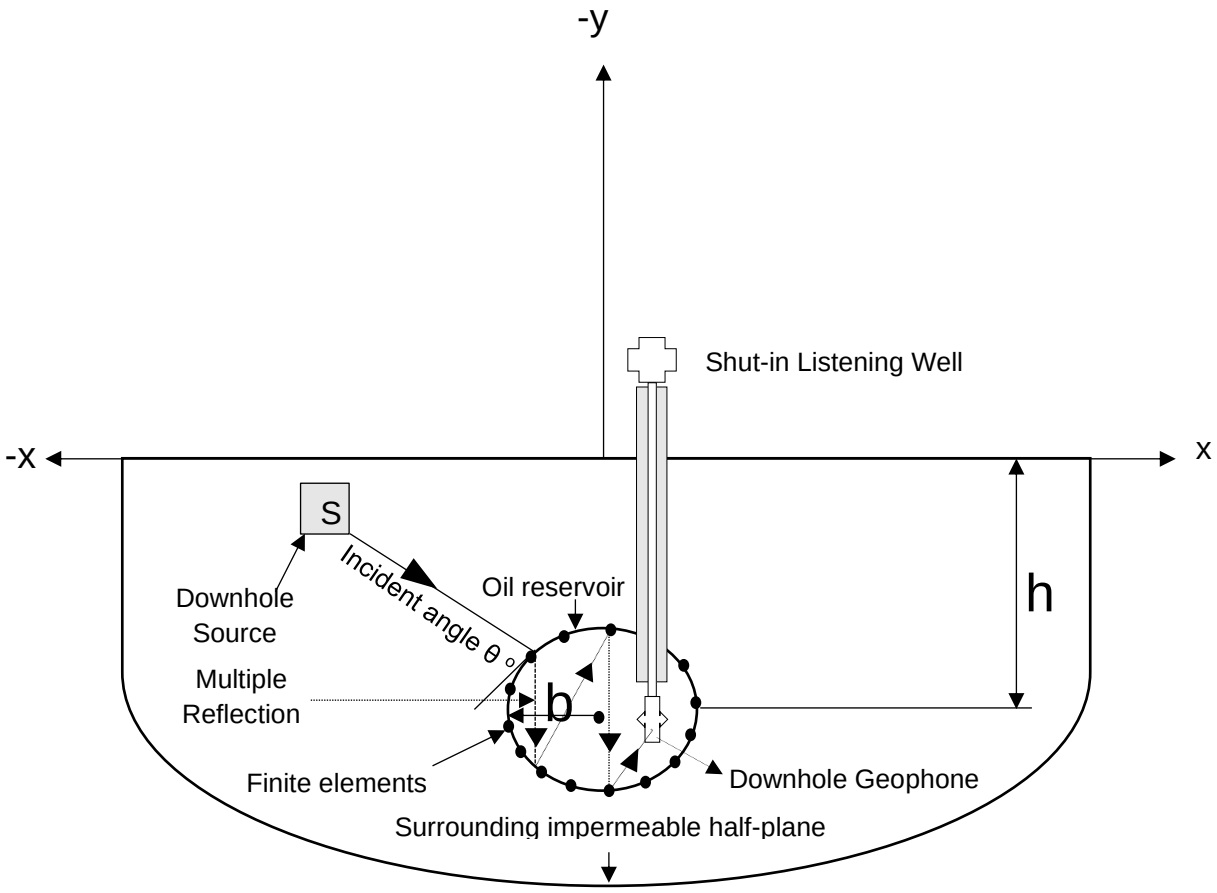

Fig. 1. A half-plane-oil reservoir model subjected to P-waves

The number of poroelastic layers is expressed by the subscript $Npls$. T(s) specifies the entire duration of the seismic wave stimulation. The motion of the impermeable elastic solid layers is denoted by $u_a(x,t)$, and the motion of the poroelastic rock matrix is expressed by $u_b(x,t)$. The relative motion between the rock matrix and pore-fluid displacement is denoted by $w(x,t)$. Furthermore, the underlying PDEs are limited to boundary conditions and the truncation interface [16,41].

The seismic stress excitation boundary condition σ (N/m^2) can be expressed by Eq. (4), and the truncation interface condition with the P-wave velocity (c) can be described by Eq. (5). Eq. (6) is the P-wave velocity.

$$\left(\left(\lambda(0)+2\mu(0)\right)\frac{\partial u_a}{\partial x}(0,t)\right)=-\sigma, \qquad t\in(0,T), \tag{4}$$

$$\frac{\partial u_a}{\partial x}(L,t)+\frac{1}{c(L)}\frac{\partial u_a}{\partial t}(L,t)=0, \qquad t\in(0,T), \tag{5}$$

$$c=\sqrt{\frac{\lambda+2\mu+\alpha^2Q}{\rho}} \tag{6}$$

The zero initial conditions are also incorporated in the underlying wave physics Eq. (7).

$$u_a(x,0)=0, \quad u_b(x,0)=0, \quad w(x,0)=0, \quad \frac{\partial u_a}{\partial t}(x,0)=0, \tag{7}$$

$$\frac{\partial u_b}{\partial t}(x,0)=0,\ \frac{\partial w}{\partial t}(x,0)=0, \qquad x\in\Omega, \tag{8}$$

Eq. (1), Eq. (2) and Eq. (3) were coupled at the boundary between the elastic solid formation and the poroelastic oil reservoir by the associated initial boundary conditions [17,42].

$$u_a|_{x_i^-}=u_b|_{x_i^+}, \qquad i=p \qquad u_a|_{x_i^+}=u_b|_{x_i^-}, \qquad i=(p+Npls), \tag{9}$$

$$\left((\lambda+2\mu)\frac{\partial u_a}{\partial x}\right)|_{x_i^-}=\left((\lambda+2\mu+\alpha^2Q)\frac{\partial u_b}{\partial x}+\alpha Q\frac{\partial w}{\partial x}\right)|_{x_i^+},\ \ i=p \tag{10}$$

$$\left((\lambda+2\mu)\frac{\partial u_a}{\partial x}\right)|_{x_i^+}=\left((\lambda+2\mu+\alpha^2Q)\frac{\partial u_b}{\partial x}+\alpha Q\frac{\partial w}{\partial x}\right)|_{x_i^-},\quad i=(p+Npls), \tag{11}$$

$$w|_{x_i}=0, \qquad i=p \qquad and \qquad i=(p+Npls), \tag{12}$$

The boundary continuity conditions of the solid rock matrix motion and overall stress are represented by Eq. (9), Eq. (10) and Eq. (11). The negligible relative motion of the pore fluid at the boundaries is described by Eq. (12), which is equivalent to the zero-flux condition $\left(\frac{\partial p}{\partial x}\right)=0$. The motion and traction continuity criteria are applied at the boundary between the elastic solid formation and the poroelastic rock formations.

$$u_a|_{x_i^-}=u_a|_{x_i^+}, \qquad i=(2,\dots,(p-1)) \quad and\ \ ((p+Npls+1),\dots,Nls), \tag{13}$$

$$\left((\lambda+2\mu)\frac{\partial u_a}{\partial x}\right)|_{x_i^-}=\left((\lambda+2\mu)\frac{\partial u_a}{\partial x}\right)|_{x_i^+}, \tag{14}$$

where (Nls) depicts the total number of formation layers in the system. The continuity criteria are also applied between the boundaries of the poroelastic formation layers.

$$u_b|_{x_i^-}=u_b|_{x_i^+}, \qquad w|_{x_i^-}=w|_{x_i^+},\ i=(p-1),\dots,(p+Npls-1), \tag{15}$$

$$\left((\lambda+2\mu+\alpha^2Q)\frac{\partial u_b}{\partial x}+\alpha Q\frac{\partial w}{\partial x}\right)|_{x_i^-}=\left((\lambda+2\mu+\alpha^2Q)\frac{\partial u_b}{\partial x}+\alpha Q\frac{\partial w}{\partial x}\right)|_{x_i^+}, \tag{16}$$

$$\left(\alpha Q\frac{\partial u_b}{\partial x}+Q\frac{\partial w}{\partial x}\right)|_{x_i^-}=\left(\alpha Q\frac{\partial u_b}{\partial x}+Q\frac{\partial w}{\partial x}\right)|_{x_i^+}, \tag{17}$$

where Eq. (15) depicts the relative motion of the pore fluid and the rock matrix. Eq. (16) and Eq. (17) describe the continuity of the total stress displacement and the pore pressure.

2.2 Numerical Modelling

The related test variables s(x), and v(x), the trial parameters (functions) $u(x,t)$, and $w(x,t)$, as well as their approximations using the finite element method (FEM) are applied in the numerical model [17,42].

$$u(x,t)=\Phi^T(x)u(t), \quad w(x,t)=\psi^T(x)w(t),$$

$$s(x) = s^T\Phi(x), \quad v(x) = v^T\psi(x), \tag{18}$$

Due to the continuity assumptions of the model, $u_a(x,t)$ and $u_b(x,t)$ are combined to form $u(x,t)$. For the spatial approximation of the trial and test parameters, the shape functions are $\Phi(x)$ and $\psi(x)$. The finite element approach results in the time-dependent semi-discrete expression for the underlying wave physics [17,42].

$$K_{uu}u + K_{uw}w + C_{uu}\frac{\partial u}{\partial t} + M_{uu}\frac{\partial u^2}{\partial t^2} + M_{uw}\frac{\partial w^2}{\partial t^2} = F_u, \tag{19}$$

$$K_{wu}u + K_{ww}w + C_{ww}\frac{\partial u}{\partial t} + M_{wu}\frac{\partial u^2}{\partial t^2} + M_{ww}\frac{\partial w^2}{\partial t^2} = 0, \tag{20}$$

The matrices elements can be described in the mathematical expressions:

$$K_{uu} = \int_{\Omega\setminus\Omega_p}(\lambda+2\mu)\frac{\partial\Phi}{\partial x}\frac{\partial\Phi^T}{\partial x}dx + \int_{\Omega_p}(\lambda+2\mu+\alpha^2Q)\frac{\partial\Phi}{\partial x}\frac{\partial\Phi^T}{\partial x}dx,\ K_{uw} = \int_{\Omega_p}(\alpha Q)\frac{\partial\Phi}{\partial x}\frac{\partial\psi^T}{\partial x}dx,$$

$$K_{wu} = \int_{\Omega_p}(\alpha Q)\frac{\partial\psi}{\partial x}\frac{\partial\Phi^T}{\partial x}dx,\ \ K_{ww} = \int_{\Omega_p}Q\frac{\partial\psi}{\partial x}\frac{\partial\psi^T}{\partial x}dx,\ \ C_{uu} = \frac{(\lambda+2\mu)}{c}\,\Phi(L)\Phi(L)^T,$$

$$C_{ww} = \int_{\Omega_p}\frac{1}{k}\psi\psi^T dx,\quad M_{uu} = \int_{\Omega}\rho\Phi\Phi^T\,dx,\quad M_{uw} = \int_{\Omega}\rho_f\Phi\psi^T\,dx,$$

$$M_{wu} = \int_{\Omega}\rho_f\psi\Phi^T\,dx,\quad M_{ww} = \int_{\Omega_p}\frac{\rho_f}{n}\psi\psi^T dx, \tag{21}$$

The time-dependent discrete formulation in Eq. (22) is the combination of Eq. (19), and Eq. (20).

$$M\frac{\partial^2 st(t)}{\partial t^2} + C\frac{\partial st(t)}{\partial t} + Kst(t) = f_{st}, \tag{22}$$

We use Newmark [43] implicit time integration to compute the semi-discrete expression of Eq. (22). By solving Eq. (22) at each time step, the discrete solutions due to the seismic wave excitation can be written in Eq. (23) [17,42].

$$\left[M + C\frac{\Delta t}{2} + K\frac{(\Delta t)^2}{4}\right]\frac{\partial^2 st_{(i+1)}}{\partial t^2} = f_{st_{(i+1)}} - C\left[\frac{\partial st_{(i)}}{\partial t} + \frac{\partial^2 st_{(i)}}{\partial t^2}\frac{\Delta t}{2}\right] - K\left[st_{(i)} + \frac{\partial st_{(i)}}{\partial t}(\Delta t) + \frac{\partial^2 st_{(i)}}{\partial t^2}\frac{(\Delta t)^2}{4}\right], \tag{23}$$

where (i) and $(i+1)$ represent the analysis of the nodal vectors at the $i-th$ and $(i+1)-th$ time steps, respectively, and Δt is the time step interval. The discretized Eq. (23) was implemented in MATLAB (2022b).

Seismic waves traveling in heterogeneous porous media cause crossflow at the interface between high and low permeability layers by creating fluid differential pressure [23,26]. Generally, wave-induced fluid flow (WIFF) affects wave transmission properties, and thus the behavior of reflection coefficients [44]. The main noticeable effect is that the reflection parameters are frequency dependent, which is referred to as reflection dispersion. Understanding the poroelastic reflection patterns (Figure 1), which are considered to have the capability to describe reservoir characteristics including saturation level and flow conditions. The current study plays a significant role in assessing the effect of WIFF on reflection coefficient characteristics within heterogeneous reservoir rocks [44]. In heterogeneous rock formations, where the impacts of elastic wave attenuation and velocity

dispersion become increasingly significant, it is crucial to discern the poroelastic reflection characteristics. Viscosity degradation in partially saturated reservoir rock or fully saturated heterogeneous rock is mostly due to internal equilibration, which occurs when fluid flows from the more elastic high-pressure areas to the considerably low-pressure zones. Local flow can be classified as mesoscopic, or squirt flow based on model size heterogeneities [28,45]. Squirt flow usually takes place at the microscopic level, but the mesoscopic flow is induced by inhomogeneities on a dimension (scale) that is significantly bigger than the average pore diameter but shorter than the macroscopic wavelength [28,44-46]. At the ultrasonic frequency range, squirt flow is generally believed to be significant, while the mesoscopic flow is widely observed to be the principal mechanism causing wave-induced fluid attenuation in the seismic frequency range [28,46]. Regarding the effects of local flow on reflection coefficients, the combined model of the Huh crossflow, and the Carcione analytical formulation of mesoscopic flow in poroelastic media are employed to study oil recovery in the oil reservoir [23,28,47]. The maximum attenuation frequency of the mesoscopic flow can be estimated using Eq. (24).

$$f_M \approx \kappa K_f/(\phi\eta t_o^2), \tag{24}$$

where M stands for mesoscopic wave propagation; k(md) is the rock permeability; K_f (GPa) is the fluid bulk modulus; η(cp) is the fluid viscosity; ϕ(%) is the rock porosity; and t_o(m) is the size of the patches. The maximum attenuation frequency of squirt flow can be calculated in the form [28,47].

$$f_{SF} \approx (z/R)^2 K_f/\eta, \tag{25}$$

where SF denotes the squirt flow; z(m) is the crack thickness; R(m) is the crack length; z/R is the crack thickness-to-crack length ratio in the porous media; K_f(GPa) is the fluid bulk modulus; and η(cp) is the fluid viscosity [28].

A simplified two-layer reservoir prototype was investigated to effectively estimate the quantity of crossflow in a heterogeneous waterflood oil reservoir (Figure 2) [23,28]. The system equations guide both the fluid flow and rock displacement induced by seismic excitation. The problems can be solved for simplified reservoir conditions to evaluate the potential of bypassed oil EOR in the low-permeability area. We focus on a generalized model where the high-permeability formation is approaching water flooding residual oil saturation (S_{orw}) and the low-permeability formation has an oil saturation level closer to the initial oil saturation (S_{oi}), (greater than S_{orw}) [23]. For the sake of simplicity, we presume that (S_{o1}) and (S_{o2}) are constant and there is no water injection during seismic wave excitation. Seismic vibrations are transmitted to the reservoir region vertically and uniformly in the x-direction. A seismic load that generates fluid flow in the two layers model is the normal stress. According to the crossflow model between the two reservoir layers, the rate of oil saturation change due to the crossflow between layers can be written in Eq. (26) [23].

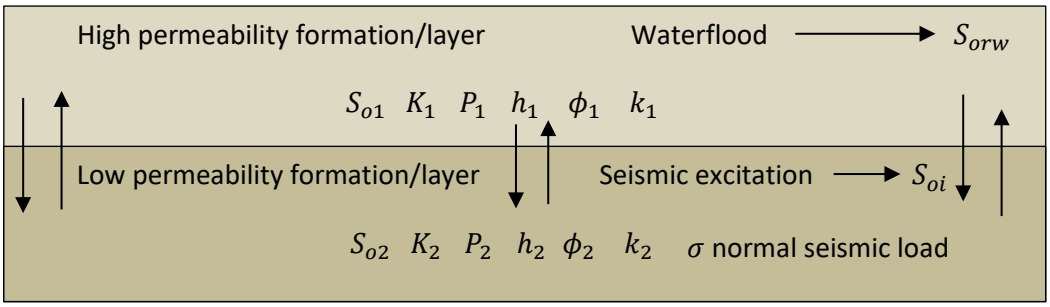

Fig. 2. Illustrates the modified two-layer reservoir prototype using the normal stress wave (σ) [23]

$$\frac{\partial S_{oi}}{\partial t} = \left(\frac{\sigma_a \omega}{\phi_1}\right)\left[\frac{\frac{iD_o\left(\frac{A_2}{M_1}-\frac{A_1}{M_2}\right)}{h_1}}{i\omega A_1 A_2 - D_T\left(\frac{A_2}{h_1}+\frac{A_1}{h_2}\right)}\right] e^{i\omega t}, \tag{26}$$

$$A = \phi\left(\frac{S_w}{Kw}+\frac{S_o}{K_o}\right)+\frac{1}{M}, \tag{27}$$

$$D_T = \frac{2}{\frac{2h_v}{\lambda_{Tv}}+\frac{h_1}{\lambda_{T1}}+\frac{h_2}{\lambda_{T2}}}, \qquad D_o = \frac{2}{\frac{2h_v}{\lambda_{ov}}+\frac{h_1}{\lambda_{o1}}+\frac{h_2}{\lambda_{o2}}}, \tag{28}$$

where h_1 is the thickness of layer 1; h_2 is the thickness of layer 2; h_v is the thickness of thin skin between the two layers; λ_{T1} is the total mobility of layer 1; λ_{T2} is the total mobility of layer 2; λ_{o1} is the oil-phase mobility of layer 1; λ_{o2} is the oil-phase mobility of layer 2; λ_{Tv} is the total mobility of the thin skin; λ_{ov} is the oil-phase mobility of the thin skin; A_1 and A_2 are the effective compressibility of layer 1 and layer 2; D_T is the effective total transmissibility; D_o is the effective oil transmissibility between two layers; M_1 is the rock modulus of layer 1; M_2 is the rock modulus of layer 2; S_{w1} is the water saturation of layer 1; S_{w2} is the water saturation of layer 2; S_{o1} is the oil saturation of layer 1; S_{o2} is the oil saturation of layer 2; ϕ_1 is the porosity of layer 1, and ϕ_2 is the porosity of layer 2.

2.3 Numerical Experiment

In a half-plane model, we consider a circular geometrical representation of an oil reservoir. A source of excitation is in the half-plane medium (Figure 1) [28]. Orbital vibrators (sources) can induce compressional (P) and shear (SH and SV) waves at amplitudes and frequencies that can be optimized to improve fluid flow through porous media [48]. The porosity and permeability of the porous media serve as the primary determinants of how fluid dynamics will be characterized [49]. According to the literature review, the fluid system is significantly impacted by phenomena including microrotation, porous media, and viscoelastic fluid [50]. The behavior and motion of fluid molecules and particles via packed beds, perforated plates, and filter sheets are studied using a porous medium model [51]. The surrounding layer in the half-plane is an impermeable elastic rock formation. High-permeability and low-permeability layers, both of which are fluid-saturated porous and permeable rock formations, have the same thickness in the heterogeneous oil reservoir (Figure 2). We focus on the impact of seismic (P-wave) excitation on the instantaneous oil transfer rate in the mature oil reservoir. We presume that water flooding operation within high permeability layer 1 swept most of the oil from the initial oil saturation (S_{oi}), to residual waterflood oil saturation (S_{orw}), and bypassed oil in the low permeability layer 2 with the oil saturation (S_{o2}) closer to the initial oil saturation (S_{oi}). The skin effect between the formation layers is negligible. The impermeable and poroelastic

layers are discretized using the quadratic element. For a forward wave excitation, the observation period lasts for 10 seconds. We validated the numerical poroelastic model results with the elastic model [17,42]. The fluid and rock properties used in the numerical study are presented in Table 1 [17,28].

Table 1
Properties of the fluid and rock used

Parameter	Symbol	Value	Unit
Density of formation Brine	ρ_w	1050	Kg/m^3
Density of Oil	ρ_o	860	Kg/m^3
Density of poroelastic solid	ρ_p	1770	Kg/m^3
Density of elastic solid	ρ_s	2000	Kg/m^3
Bulk modulus of drained solid layer 1	K_1	3.9x10^9	N/m^2
Bulk modulus of drained solid layer 2	K_2	6.0x10^9	N/m^2
Bulk modulus of undrained solid layer 1	K_{d1}	5.0x10^9	N/m^2
Bulk modulus of undrained solid layer 2	K_{d2}	3.5x10^9	N/m^2
Bulk modulus of formation Brine	K_b	3.0x10^9	N/m^2
Bulk modulus of oil	K_o	6.7x10^8	N/m^2
Viscosity of formation Brine	μ_w	1.0x10^{-3}	Ns/m^2
Viscosity of oil	μ_o	5.0x10^{-3}	Ns/m^2
Seismic Stress	σ	10	N/m^2
Permeability of layer 1	k_1	4.44x10^{-13}	m^2
Permeability of layer 2	k_2	1.97x10^{-13}	m^2
Fluid mobility in layer 1	λ_1	1.45x10^{-10}	m^{3}s/kg
Fluid mobility in layer 2	λ_2	3.94x10^{-11}	m^{3}s/kg
Irreducible water saturation	S_{wi}	0.2	%
Reservoir thickness	t	100	m
High permeability area thickness	h_1	50	m
Low permeability area thickness	h_2	50	m
Excitation frequency	f	3.0	Hz

3. Results and Discussions

3.1 Vertical Displacement

In this section, the findings of the vertical displacement (rock matrix and fluid) in a low permeability area of a heterogeneous oil reservoir are presented. The effects of observation radius (r_o) on fluid and solid matrix displacement amplitudes in the poroelastic model are evaluated as a function of time. The wellbore radius (r_w) is 0.06m and the oil reservoir radius (b) is 500m.

3.1.1 The effect of observation radius

At the observation radius of 50m, it was observed that the fluid displacement amplitude declined very rapidly with observation time. Since the fluid pulse attenuates very quickly (exponential decay) due to the tortuosity of the reservoir rock pore space. Pressure diffusivity, in principle, governs the propagation of fluid pressure waves; as fluid viscosity or compressibility rises, and/or permeability declines, the dispersion rises, and the fluid displacement amplitude attenuates more abruptly (Figure 3) [42]. The propagation of fluid vibrations via the pore space is greatly attenuated due to the tortuosity of the pore space, while the propagation of elastic rock matrix displacement inside the reservoir rock appears to be more significant (Figure 4). When a seismic vibration is delivered using downhole technology, the reservoir rock surface is compressed, and the displacement propagates

across the matrix of the reservoir rock, stimulating both the matrix and the pore fluid. The progression of the vertical displacements over time is depicted in Figure 4.

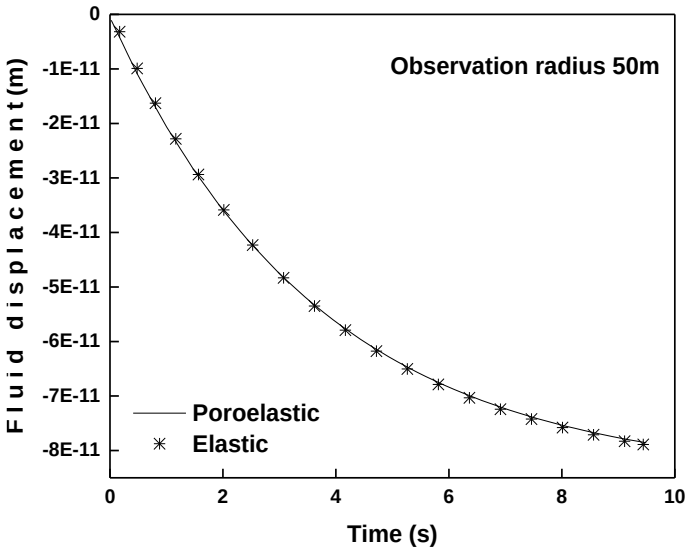

Fig. 3. Illustrates the displacement fields of pore fluid oscillations

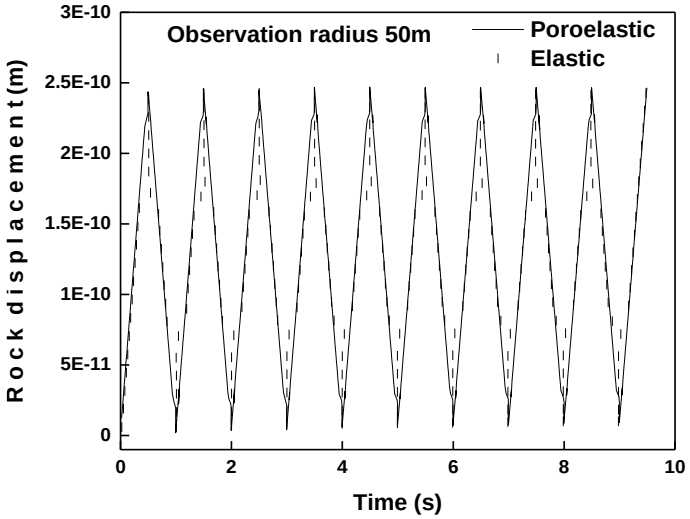

Fig. 4. Illustrates the displacement fields of rock matrix oscillations

The seismic stress creates a compressional wave that travels vertically through the oil reservoir layers. This compressional wave is reflected multiple times intermittently in the oil reservoir within the observation period of 10 seconds and the downhole geophones recorded the fluid and rock matrix displacement amplitudes. Thus, the matrix displacement amplitude shows a sustainable zigzag displacement pattern [52,53]. The condition of the reservoir and the amount of the stress wave load determine the amplitude of the displacement. It is demonstrated that the amplitude of pore fluid displacement (Figure 3) is smaller than the magnitude of rock matrix displacement (Figure 4) at the same observation radius. The magnitude of the pore fluid displacement diminished in a slightly linear decay pattern when the observation radius was increased to 100m towards the reservoir boundary (Figure 5). It was demonstrated that the displacement amplitude decay is slower at observation radii of 50 m than at 100 m. Since fluid displacement distribution in the reservoir is

diffusive, the magnitude of the fluid oscillation declines with distance from the wellbore, which is mostly determined by the pressure diffusivity factor. The higher the compressibility of the pore fluids, the smaller the fluid displacement amplitude. The vertical displacement of the rock matrix expanded as the reservoir observation radius increased to 100m (Figure 6).

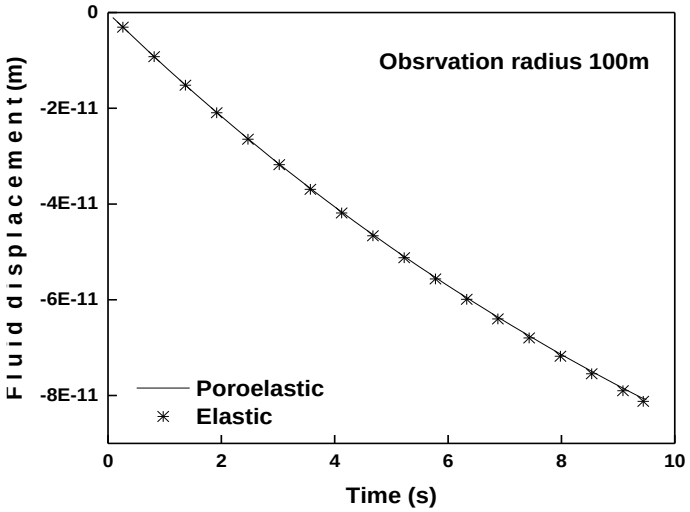

Fig. 5. Illustrates the displacement fields of pore fluid oscillations

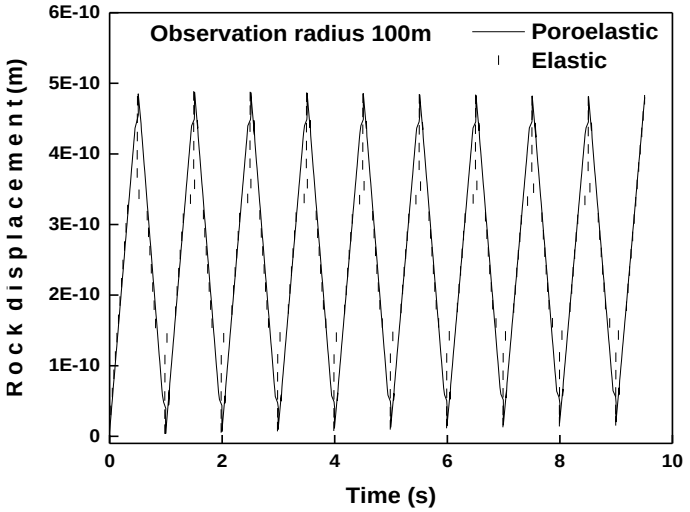

Fig. 6. Illustrates the displacement fields of rock matrix oscillations

The vertical displacement of the rock matrix retains a zigzag displacement trend throughout the observation period. The displacement amplitude of the two-phase conditions is greater than that of the single cases since seismic frequency signals can reflect long-term behavior. The displacement of the rock matrix is observed to rise as the observation radius moves nearer the reservoir boundary and away from the wellbore radius. The stress wave imparted to the solid skeleton is much more effectively transmitted to the pore fluids in a multiphase condition, whereas the influence caused by the fluid-fluid contact is relatively small to be considered. The pore fluid displacement amplitude decreased linearly in a straight-line trend when the observation radius was raised to 200m, as shown in Figure 7.

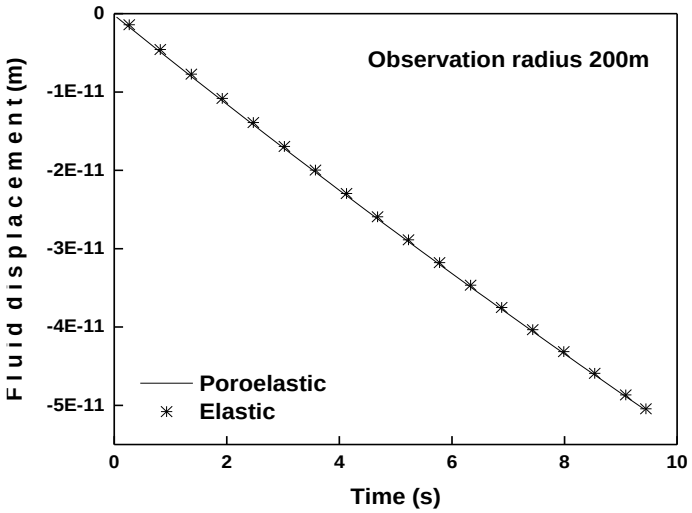

Fig. 7. Illustrates the displacement fields of pore fluid oscillations

This is due to the greater compressibility of the reservoir formation as the radius approaches the boundary of the oil reservoir. The rock matrix displacement increased in a zig-zag pattern as the observation radius increased by 200m approaching the oil reservoir boundary (Figure 8). The results showed that the diffusion of time-domain fluid displacement oscillations across the pore space was highly attenuated and that the propagation of rock matrix displacement in the low permeability area could be more effective during crossflow in the heterogeneous reservoir. The porosity of the low permeability layer ϕ_2, the diameter of the patches d, and the aspect ratio h/R, were considered as 0.23%, 0.2m, and 0.001 respectively.

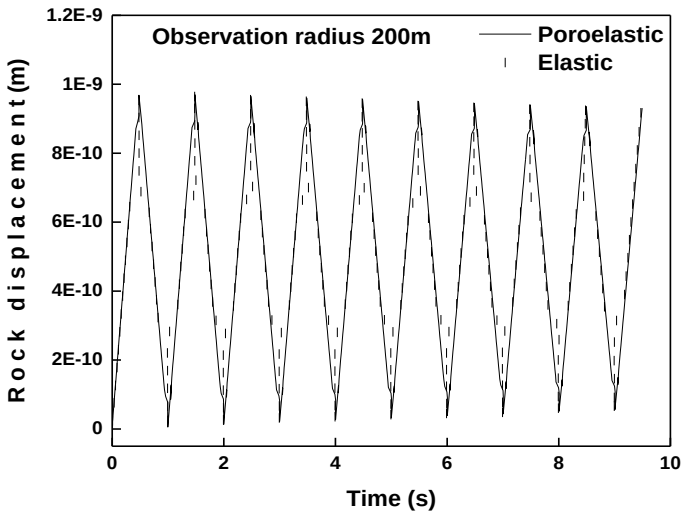

Fig. 8. Illustrates the displacement fields of solid rock oscillations

The predicted attenuation findings for mesoscopic flow frequency (f_m) and squirt flow frequency (f_{sf}) are 3.0 Hz, and f_{SF}= 3.0 MHz, respectively. The process of attenuation in the low permeability layer of a heterogeneous oil reservoir is mesoscopic, whereas the squirt flow peak attenuation frequency is beyond the seismic frequency band (ultrasonic). It was finally demonstrated that the trapped oil bypassed by the water flooding phase and nevertheless remaining in the low-permeability region of the heterogeneous oil reservoir could be displaced to the high-permeability region by

seismic-induced crossflow. Figure 9 shows the prediction of the transient oil saturation variation caused by crossflow between the layers in the oil reservoir. The crossflow at 3.0 Hz mesoscopic attenuation frequency demonstrated a 2.5% instantaneous oil transfer rate (recovery rate) of bypassed oil by seismic waves (Figure 9).

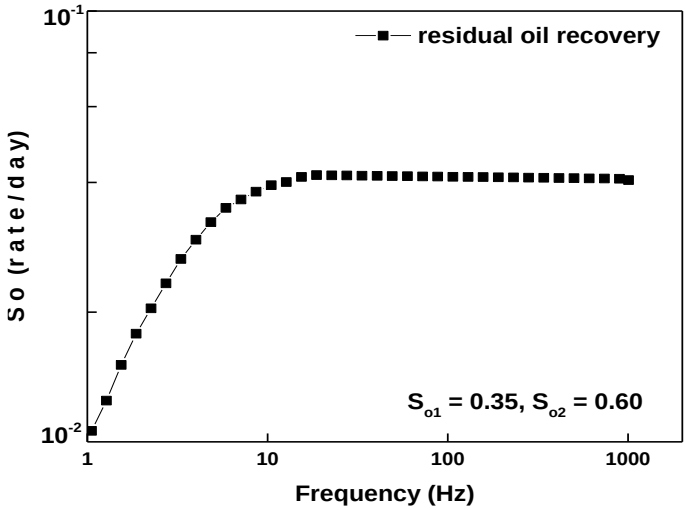

Fig. 9. illustrates the oil transfer rate within two layers (scaled with σ_a) in terms of mesoscopic frequency and combinations of oil saturations [23]

The mesoscopic frequency can be used to monitor the recovery rate of the bypassed oil in the reservoir during seismic excitation at different saturation combinations of formation layers. Seismic excitation can also be combined with water flooding to recover more oil from both high and low-permeability areas. The pore fluid displacement response in the low permeability layer decay very rapidly as the seismic wave travels through a heterogeneous oil reservoir, while the matrix displacement effectively propagates and sustains crossflow across the layers and perhaps forces oil from the low-permeability formation into the wellbore.

4. Conclusion

The current study uses a downhole seismic source in a half-plane model to explore the performance of elastic wave propagation in a low-permeability formation of a heterogeneous oil reservoir. As the observation radius approaches the boundary of the oil reservoir, the rock matrix displacement magnitude tends to have stronger wave energy than the fluid displacement amplitude in the low permeability zone. Time-domain rock matrix displacement appears to cause crossflow within the formation layers, which can dislodge oil from the rock matrix. The instantaneous oil transfer can be recovered (2.5 % rate per day) at the mesoscopic frequency of 3.0 Hz due to the increased sweep of the residual oil caused by the crossflow at the boundary of the low-permeability zone bypassed by the water flooding approach. Seismic wave EOR can be combined with water flooding to recover more oil for both low and high-permeability regions of the mature oil reservoir. Therefore, the peak mesoscopic frequency can be employed as one of the indicators used to evaluate oil recovery in heterogeneous oil reservoirs.

Acknowledgment

This work was supported by the FRG Project at the Universiti Teknologi PETRONAS with Grant No: 015LC0-447.

References

[1] Yakasai, Faruk, Mohd Zaidi Jaafar, Sulalit Bandyopadhyay, and Augustine Agi. "Current developments and future outlook in nanofluid flooding: A comprehensive review of various parameters influencing oil recovery mechanisms." *Journal of Industrial and Engineering Chemistry* 93 (2021): 138-162. https://doi.org/10.1016/j.jiec.2020.10.017

[2] Tapia, John Frederick D., Jui-Yuan Lee, Raymond E. H. Ooi, Dominic C. Y. Foo, and Raymond R. Tan. "Optimal CO_2 allocation and scheduling in enhanced oil recovery (EOR) operations." *Applied Energy* 184 (2016): 337-345. https://doi.org/10.1016/j.apenergy.2016.09.093

[3] Druetta, P., P. Raffa, and F. Picchioni. "Chemical enhanced oil recovery and the role of chemical product design." *Applied Energy* 252 (2019): 113480. https://doi.org/10.1016/j.apenergy.2019.113480

[4] Doman, E. L. "World Energy Demand and Economic Outlook." In *International Energy Outlook*, 2016.

[5] Kakati, Abhijit, Ganesh Kumar, and Jitendra S. Sangwai. "Low salinity polymer flooding: effect on polymer rheology, injectivity, retention, and oil recovery efficiency." *Energy & Fuels* 34, no. 5 (2020): 5715-5732. https://doi.org/10.1021/acs.energyfuels.0c00393

[6] Adeyemi, Idowu, Mahmoud Meribout, and Lyes Khezzar. "Recent developments, challenges, and prospects of ultrasound-assisted oil technologies." *Ultrasonics Sonochemistry* 82 (2022): 105902. https://doi.org/10.1016/j.ultsonch.2021.105902

[7] Nhut, Le Minh, Ha Nguyen Minh, and Luan Nguyen Thanh. "The Effective and Exergy Efficiency of Multi-Pass Solar Air Collector with Longitudinal Fins: Analysis and Optimization." *Journal of Advanced Research in Fluid Mechanics and Thermal Sciences* 102, no. 2 (2023): 42-65. https://doi.org/10.37934/arfmts.102.2.4265

[8] Al Rizeiqi, Nasser Mohammed, Nasser Al Rizeiqi, and Ali Nabavi. "Potential of Underground Hydrogen Storage in Oman." *Journal of Advanced Research in Applied Sciences and Engineering Technology* 27, no. 1 (2022): 9-31. https://doi.org/10.37934/araset.27.1.931

[9] Tveiten, Ole Gunnar. "Recycling CO_2 for EOR? Why Not?." *Journal of Petroleum Technology*. February 1, 2023. https://jpt.spe.org/recycling-co2-for-eor-why-not.

[10] Abdullahi, M. B., S. R. Jufar, S. Kumar, T. M. Al-shami, and B. M. Negash. "Synergistic effect of Polymer-Augmented low salinity flooding for oil recovery efficiency in Illite-Sand porous media." *Journal of Molecular Liquids* 358 (2022): 119217. https://doi.org/10.1016/j.molliq.2022.119217

[11] Sun, Qian, Albertus Retnanto, and Mahmood Amani. "Seismic vibration for improved oil recovery: A comprehensive review of literature." *International Journal of Hydrogen Energy* 45, no. 29 (2020): 14756-14778. https://doi.org/10.1016/j.ijhydene.2020.03.227

[12] Rahman, Musfika, and Iskandar Dzulkarnain. "RSM for Modelling the CO_2 Effect in the Interfacial Tension Between Brine and Waxy Dulang Crude Oil During LSW-WAG EOR." *Journal of Advanced Research in Fluid Mechanics and Thermal Sciences* 85, no. 2 (2021): 159-174. https://doi.org/10.37934/arfmts.85.2.159174

[13] Jeong, Chanseok, Chun Huh, and Loukas F. Kallivokas. "On the feasibility of inducing oil mobilization in existing reservoirs via wellbore harmonic fluid action." *Journal of Petroleum Science and Engineering* 76, no. 3-4 (2011): 116-123. https://doi.org/10.1016/j.petrol.2011.01.005

[14] Hamidzadeh, Hamid R., Liming Dai, and Reza N. Jazar. *Wave propagation in solid and porous half-space media*. Berlin: Springer, 2014. https://doi.org/10.1007/978-1-4614-9269-6

[15] Wooden, Bill. "Technology Update: Seismic Stimulation: An Eco-Friendly, Effective EOR Alternative." *Journal of Petroleum Technology* 70, no. 08 (2018): 21-23. https://doi.org/10.2118/0818-0021-JPT

[16] Dai, Liming, and Yihe Zhang. "Effects of low frequency external excitation on oil slug mobilization and flow in a water saturated capillary model." *Petroleum* 5, no. 4 (2019): 375-381. https://doi.org/10.1016/j.petlm.2019.03.001

[17] Jeong, Chanseok, Loukas F. Kallivokas, Chun Huh, and Larry W. Lake. "Estimation of oil production rates in reservoirs exposed to focused vibrational energy." In *SPE Improved Oil Recovery Symposium*. OnePetro, 2014. https://doi.org/10.2118/169079-MS

[18] Kurawle, Irfan, Mohit Kaul, Nakul Mahalle, Vickey Carvalho, Neelendra Nath, and Zohaib Amin. "Seismic EOR-the optimization of aging waterflood reservoirs." In *SPE Offshore Europe Oil and Gas Conference and Exhibition*. OnePetro, 2009. https://doi.org/10.2118/123304-MS

[19] Abdullahi, Mohammed Bashir, Kourosh Rajaei, Radzuan Junin, and Ali Esfandyari Bayat. "Appraising the impact of metal-oxide nanoparticles on rheological properties of HPAM in different electrolyte solutions for enhanced oil

recovery." *Journal of Petroleum Science and Engineering* 172 (2019): 1057-1068. https://doi.org/10.1016/j.petrol.2018.09.013

[20] Kang, Pan-Sang, Jong-Se Lim, and Chun Huh. "Temperature dependence of relaxation time of hydrolyzed polyacrylamide solution for enhanced oil recovery." *Journal of Industrial and Engineering Chemistry* 78 (2019): 257-264. https://doi.org/10.1016/j.jiec.2019.06.004

[21] Kouznetsov, O. L., E. M. Simkin, G. V. Chilingar, and S. A. Katz. "Improved oil recovery by application of vibro-energy to waterflooded sandstones." *Journal of Petroleum Science and Engineering* 19, no. 3-4 (1998): 191-200. https://doi.org/10.1016/S0920-4105(97)00022-3

[22] Furman, K., S. Miftakhov, M. Nazyrov, R. Nefedov, V. Zamakhaev, and A. Andrianov. "Increasing wells injectivity and productivity by seismic and seismo-chemical stimulation." In *SPE EOR Conference at Oil and Gas West Asia*. OnePetro, 2018. https://doi.org/10.2118/190456-MS

[23] Huh, Chun. "Improved oil recovery by seismic vibration: a preliminary assessment of possible mechanisms." In *International Oil Conference and Exhibition in Mexico*. OnePetro, 2006. https://doi.org/10.2118/103870-MS

[24] Louhenapessy, Stevy Canny, and Tutuka Ariadji. "The effect of type waves on vibroseismic implementation of changes properties of rock, oil viscosity, oil compound composition, and enhanced oil recovery." *Petroleum Research* 5, no. 4 (2020): 304-314. https://doi.org/10.1016/j.ptlrs.2020.05.001

[25] Kostrov, Sergey, and William Wooden. "Possible mechanisms and case studies for enhancement of oil recovery and production using in-situ seismic stimulation." In *SPE Symposium on Improved Oil Recovery*. OnePetro, 2008. https://doi.org/10.2118/114025-MS

[26] Allahverdiyev, Parviz Qadir. "Improved sweep efficiency through seismic wave stimulation." *PhD diss., The University of Texas at Austin*, 2012.

[27] Jeong, C., L. F. Kallivokas, S. Kucukcoban, W. Deng, and A. Fathi. "Maximization of wave motion within a hydrocarbon reservoir for wave-based enhanced oil recovery." *Journal of Petroleum Science and Engineering* 129 (2015): 205-220. https://doi.org/10.1016/j.petrol.2015.03.009

[28] Abdullahi, Mohammed Bashir, Shiferaw Regassa Jufar, S. Kumar, Tareq Mohammed Al-shami, and M. D. Le. "Characteristics of SH-wave propagation during oil reservoir excitation using BEM formulation in half-plane model representation." *International Journal of Rock Mechanics and Mining Sciences* 162 (2023): 105303. https://doi.org/10.1016/j.ijrmms.2022.105303

[29] Simkin, E. M., and M. L. Surguchev. "Advanced vibroseismic technique for water flooded reservoir stimulation, mechanism and field tests results." In *IOR 1991-6th European Symposium on Improved Oil Recovery*, pp. cp-44. European Association of Geoscientists & Engineers, 1991.

[30] Beresnev, Igor A. "Theory of vibratory mobilization on nonwetting fluids entrapped in pore constrictions." *Geophysics* 71, no. 6 (2006): N47-N56. https://doi.org/10.1190/1.2353803

[31] Beckham, Richard E., Amr I. Abdel-Fattah, Peter M. Roberts, Reem Ibrahim, and Sowmitri Tarimala. "Mobilization of colloidal particles by low-frequency dynamic stress stimulation." *Langmuir* 26, no. 1 (2010): 19-27. https://doi.org/10.1021/la900890n

[32] Roberts, Peter M., and Amr I. Abdel-Fattah. "Seismic stress stimulation mobilizes colloids trapped in a porous rock." *Earth and Planetary Science Letters* 284, no. 3-4 (2009): 538-543. https://doi.org/10.1016/j.epsl.2009.05.017

[33] Roberts, Peter M., Igor B. Esipov, and Ernest L. Majer. "Elastic wave stimulation of oil reservoirs: Promising EOR technology?." *The Leading Edge* 22, no. 5 (2003): 448-453. https://doi.org/10.1190/1.1579578

[34] Roberts, Peter M., Arvind Sharma, Venkatesh Uddameri, Matthew Monagle, Don E. Dale, and Lee K. Steck. "Enhanced DNAPL transport in a sand core during dynamic stress stimulation." *Environmental Engineering Science* 18, no. 2 (2001): 67-79. https://doi.org/10.1089/10928750151132230

[35] Vogler, Eric T., and Constantinos V. Chrysikopoulos. "An experimental study of acoustically enhanced NAPL dissolution in porous media." *AIChE Journal* 50, no. 12 (2004): 3271-3280. https://doi.org/10.1002/aic.10221

[36] Spanos, Tim, B. Davidson, M. Dusseault, D. Shand, and M. Samaroo. "Pressure pulsing at the reservoir scale: a new IOR approach." *Journal of Canadian Petroleum Technology* 42, no. 02 (2003). https://doi.org/10.2118/03-02-01

[37] Iassonov, Pavel P., and Igor A. Beresnev. "A model for enhanced fluid percolation in porous media by application of low-frequency elastic waves." *Journal of Geophysical Research: Solid Earth* 108, no. B3 (2003). https://doi.org/10.1029/2001JB000683

[38] Li, Wenqing, R. Dennis Vigil, Igor A. Beresnev, Pavel Iassonov, and Robert Ewing. "Vibration-induced mobilization of trapped oil ganglia in porous media: Experimental validation of a capillary-physics mechanism." *Journal of Colloid and Interface Science* 289, no. 1 (2005): 193-199. https://doi.org/10.1016/j.jcis.2005.03.067

[39] Beresnev, Igor, William Gaul, and R. Dennis Vigil. "Direct pore-level observation of permeability increase in two-phase flow by shaking." *Geophysical Research Letters* 38, no. 20 (2011). https://doi.org/10.1029/2011GL048840

[40] Beresnev, Igor A., and Wen Deng. "Viscosity effects in vibratory mobilization of residual oil." Geophysics 75, no. 4 (2010): N79-N85. https://doi.org/10.1190/1.3429999

[41] Deng, Wen, and M. Bayani Cardenas. "Dynamics and dislodgment from pore constrictions of a trapped nonwetting droplet stimulated by seismic waves." *Water Resources Research* 49, no. 7 (2013): 4206-4218. https://doi.org/10.1002/wrcr.20335
[42] Jeong, Chanseok. "On an inverse-source problem for elastic wave-based enhanced oil recovery." *PhD diss., The University of Texas at Austin*, 2011.
[43] Newmark, Nathan M. "A method of computation for structural dynamics." *Journal of the Engineering Mechanics Division* 85, no. 3 (1959): 67-94. https://doi.org/10.1061/JMCEA3.0000098
[44] Zhao, Luanxiao, De-hua Han, Qiuliang Yao, Rui Zhou, and Fuyong Yan. "Seismic reflection dispersion due to wave-induced fluid flow in heterogeneous reservoir rocks." *Geophysics* 80, no. 3 (2015): D221-D235. https://doi.org/10.1190/geo2014-0307.1
[45] Müller, T., B. Gurevich, and M. Lebedev. "Seismic wave attenuation and dispersion due to wave-induced flow at mesoscopic heterogeneities-A review." *Geophysics* 75, no. 5 (2010): 75A147-75A164. https://doi.org/10.1190/1.3463417
[46] Zheng, Pei, Boyang Ding, and Xiuting Sun. "Elastic wave attenuation and dispersion induced by mesoscopic flow in double-porosity rocks." *International Journal of Rock Mechanics and Mining Sciences* 91 (2017): 104-111. https://doi.org/10.1016/j.ijrmms.2016.11.018
[47] Carcione, José M., Christina Morency, and Juan E. Santos. "Computational poroelasticity-A review." *Geophysics* 75, no. 5 (2010): 75A229-75A243. https://doi.org/10.1190/1.3474602
[48] Westermark, R. V., J. F. Brett, and D. R. Maloney. "Enhanced oil recovery with downhole vibration stimulation." In *SPE Production and Operations Symposium*. OnePetro, 2001. https://doi.org/10.2118/67303-MS
[49] Sunhazim, Nur Shamimi Amirah Md, Ummi Aqila Norhaidi, Muhammad Afiq Witri Muhammad Yazid, Fazila Mohd Zawawi, and Ummikalsom Abidin. "Characterization of fluid flow through porous media." *Journal of Advanced Research in Fluid Mechanics and Thermal Sciences* 96, no. 2 (2022): 22-32. https://doi.org/10.37934/arfmts.96.2.2232
[50] Kasim, Abdul Rahman Mohd, Laila Amera Aziz, Noor Amalina Nisa Ariffin, Mohamad Hidayad Ahmad Kamal, Iskandar Waini, Mohd Zuki Salleh, and Dennis Ling Chuan Ching. "Flow Analysis on Boundary Layer of Porous Horizontal Circular Cylinder Filled by Viscoelastic-Micropolar Fluid." *CFD Letters* 14, no. 11 (2022): 49-62. https://doi.org/10.37934/cfdl.14.11.4962
[51] Harolanuar, Muhammad Nur Hanafi, Nurul Fitriah Nasir, Hanis Zakaria, and Ishkrizat Taib. "Analysis of Fluid Flow on the N95 Facepiece Filtration Layers." *Journal of Advanced Research in Fluid Mechanics and Thermal Sciences* 100, no. 1 (2022): 172-180. https://doi.org/10.37934/arfmts.100.1.172180
[52] Li, Peng, and Martin Schanz. "Time domain boundary element formulation for partially saturated poroelasticity." *Engineering Analysis with Boundary Elements* 37, no. 11 (2013): 1483-1498. https://doi.org/10.1016/j.enganabound.2013.08.002
[53] Albers, Bettina, Stavros A. Savidis, H. Ercan Taşan, Otto von Estorff, and Malte Gehlken. "BEM and FEM results of displacements in a poroelastic column." *International Journal of Applied Mathematics and Computer Science* 22, no. 4 (2012): 883-896. https://doi.org/10.2478/v10006-012-0065-y